Multifrequency Electron Spin Resonance Spectra of a Spin-Labeled Protein Calculated from Molecular Dynamics Simulations

Deniz Sezer,[†,⊥,‡] Jack H. Freed,[§] and Benoît Roux*,[⊥]

Department of Physics, Cornell University, Ithaca, New York 14853, Department of Chemistry and Chemical Biology, Cornell University, Ithaca, New York 14853, and Department of Biochemistry and Molecular Biology, The University of Chicago, Chicago, Illinois 60637

Received September 17, 2008; E-mail: roux@uchicago.edu

Abstract: Multifrequency electron spin resonance (ESR) spectra provide a wealth of structural and dynamic information about the local environment of the spin label and, indirectly, about the spin-labeled protein. Relating the features of the observed spectra to the underlying molecular motions and interactions is, however, challenging. To make progress toward a rigorous interpretation of ESR spectra, we perform extensive molecular dynamics (MD) simulations of fully solvated T4 Lysozyme, labeled with the spin label MTSSL at positions 72 and 131. These two sites have been the object of numerous experimental studies and are generally considered as prototypical solvent-exposed sites on the surfaces of α-helices. To extend the time window afforded by the MD simulations, stochastic Markov models reflecting the dynamics of the spin label side chains in terms of their rotameric states are constructed from the trajectories. The calculated multifrequency ESR spectra are in very good agreement with experiment for three different magnetic field strengths without adjusting any parameters. During the trajectories, the spin labels interconvert among a fairly large number of conformations and display a propensity to form interactions with protein residues other than their nearest neighbors along the helix. The detailed picture of the spin label emerging from the MD simulations provides useful insight into the molecular origins of the available spectroscopic and crystallographic data.

1. Introduction

Electron spin resonance (ESR) combined with site-directed spin labeling (SDSL) is a powerful biophysical technique for probing the conformational dynamics of a protein in its native environment.[1−3] Partly owing to the high sensitivity of the technique and the relative ease with which proteins can be labeled by introducing cysteine mutations, ESR plays an increasingly important role in studies focusing on the function of membrane proteins.[4−9] When the aim is to delineate broad structural features of a protein, the interpretation of the ESR spectra is relatively straightforward. For instance, secondary structural elements can be mapped out by systematically scanning the protein by SDSL and comparing the resulting spectra. With the aid of additional paramagnetic agents, information about the overall position of the subunits of a membrane protein with respect to one another or to the membrane itself can also be obtained. However, when detailed structural and dynamic information is sought, the specific features of the spectral line shapes need to be carefully understood and interpreted. In this case, understanding the energetics and dynamics of the spin label becomes of paramount importance.

Extensive efforts have been dedicated to elucidate the microscopic factors affecting the conformation and dynamics of spin labels attached to proteins. Particularly informative are the experimental studies of the commonly used nitroxide spin label MTSSL (Figure 1, top) attached to the well-characterized protein T4 Lysozyme (T4L, Figure 1, bottom). A wealth of results, ranging from X-ray crystallography of spin-labeled T4L to X-band (9 GHz) or multifrequency ESR experiments, is now available.[10−18] From those studies, two positions, 72 and 131, respectively situated in the middle of a long and a short helix, have emerged as prototypical solvent-exposed helix surface (SEHS) sites (Figure 1, bottom). At both positions, the spin

---

† Department of Physics, Cornell University.
§ Department of Chemistry and Chemical Biology, Cornell University.
⊥ Department of Biochemistry and Molecular Biology, The University of Chicago.
‡ Present address: Institute for Physical and Theoretical Chemistry, J. W. Goethe University, 60438 Frankfurt am Main, Germany.

(1) Borbat, P. P.; Costa-Filho, A. J.; Earle, K. A.; Moscicki, J. K.; Freed, J. H. *Science* **2001**, *291*, 266.
(2) Columbus, L.; Hubbell, W. L. *TIBS* **2002**, *27*, 288.
(3) Borbat, P. P.; Freed, J. H. *Methods Enzymol.* **2007**, *423*, 52.
(4) Perozo, E.; Marien Cortes, D.; Sompornpisut, P.; Kloda, A.; Martinac, B. *Nature* **2002**, *418*, 942.
(5) Cuello, L. G.; Marien Cortes, D.; Perozo, E. *Science* **2004**, *306*, 491.
(6) Dong, J.; Guangyong, Y.; Mchaourab, H. S. *Science* **2005**, *308*, 1023.
(7) Park, S.-Y.; Borbat, P. P.; Gonzalez-Bonet, G.; Bhatnagar, J.; Pollard, A. M.; Freed, J. H.; Bilwes, A. M.; Crane, B. R. *Nat. Struct. Biol.* **2006**, *13*, 400.
(8) Borbat, P. P.; Surendhran, K.; Bortolus, M.; Zou, P.; Freed, J. H.; Mchaourab, H. S. *PLoS Biol.* **2007**, *5*, 2211.
(9) Smirnova, I.; Kasho, V.; Choe, J.-Y.; Altenbach, C.; Hubbell, W. L.; Kaback, H. R. *Proc. Natl. Acad. Sci. U.S.A.* **2007**, *104*, 16504.

(10) Mchaourab, H. S.; Lietzow, M. A.; Hideg, K.; Hubbell, W. L. *Biochemistry* **1996**, *35*, 7692.
(11) Mchaourab, H. S.; Kalai, T.; Hideg, K.; Hubbell, W. L. *Biochemistry* **1999**, *38*, 2947.
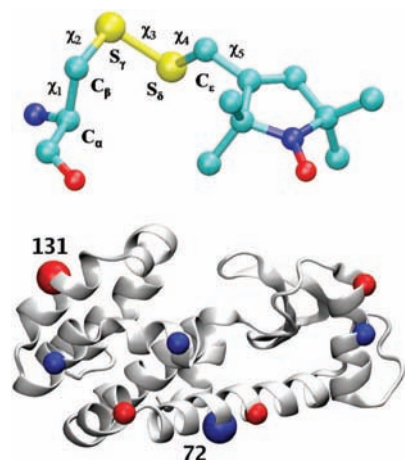
Figure 1. (Top) "Side chain" R1 resulting from linking MTSSL (1-oxyl-2,2,5,5-tetramethylpyrroline-3-methyl-methanethiosulfonate) to a cysteine through a disulfide bond. (Bottom) Cartoon representation of T4 Lysozyme. Spin labels were present simultaneously at same-color sites in simulation set 1 (blue) or 2 (red). Only the sites studied in this work are numbered.

label (R1) is not expected to be involved in tertiary contacts. The 9 GHz spectra of 72R1 and 131R1 are insensitive to alanine mutation of the neighboring $i \pm 3$ and $i \pm 4$ residues, suggesting that the spin label interacts only weakly with the rest of the helix.[2,10,11] However, the spectra also indicate that the conformational freedom of the spin label is somewhat restricted.

These observations have been rationalized in terms of the "χ_4/χ_5 model" for SEHS sites,[2,14] which assumes that the internal motion of R1 is largely limited to rotations about the last two dihedrals of the side chain (Figure 1, top). According to this model, the remaining dihedrals are effectively "locked" on the ESR time scale; the χ_3 disulfide torsion is opposed by a large energy barrier,[19] while the χ_1 and χ_2 torsions are hindered by the formation of a hydrogen bond between the sulfur atom of R1 and the backbone amide[10] or C_α.[2] Such sulfur-backbone contacts are indeed observed in a number of X-ray crystal structures of T4L with spin labels[13,15,17,18] in support of the χ_4/χ_5 model. Furthermore, the χ_4/χ_5 model offers an atomistic rationalization of the fitting parameters of the diffusional models MOMD[20] and SRLS[21,22] which can produce simulated spectra in quantitative agreement with experiments.

According to the current understanding, 72R1 and 131R1 in T4L are believed to exemplify the internal R1 dynamics at SEHS sites unaffected by tertiary contacts. The differences in the 9 GHz spectra at these two positions are thought to reflect the effect of backbone motion on the mobility of the spin-label side

chain.[14] Nevertheless, a number of issues remain. For instance, the spin label is partly disordered and somewhat unresolved in several X-ray structures, suggesting that multiple conformations are energetically accessible, a view that is encouraged also by *ab initio* computational studies,[23] and the recent crystal structure of 131R1.[18] Therefore, in spite of the extensive data available, further clarification of the spin-label dynamics at SEHS sites at the atomic level remains a significant objective.

In principle, molecular dynamics (MD) simulations could be used to shed light on this issue, providing a "virtual route" to link the atomistic dynamics to the experimental observations. In practice, this remains challenging, since very long trajectories are required to exhaustively sample the accessible conformations of the spin label and to allow an adequate relaxation of the quantal degrees of freedom,[23,24] which has prevented all-atom simulations of T4L with explicit solvent from obtaining quantitative agreement between the calculated 9 GHz spectra and experiment.[25,26] To overcome such sampling difficulties, many MD studies of spin-labeled proteins have simplified the atomic model by simulating in implicit solvent[27,28] or in vacuum at high temperatures (600 K).[29,30]

Another concern is the quality of the force fields used to generate the MD trajectories. Recently, an all-atom potential function for the nitroxide spin label R1 was developed using extensive quantum mechanical calculations.[23] Furthermore, a novel methodological framework was elaborated for the purpose of simulating ESR spectra of spin-labeled proteins from all-atom MD trajectories.[31] Within this framework, the information from multiple independent MD trajectories is employed to construct a discrete-state Markov jump model of the R1 dynamics in the space of its five dihedral angles. Using the transition probability matrix of the Markov jump model determined from the MD simulations, long stochastic trajectories including isotropic diffusional rotation are generated to simulate realistic ESR spectra.[24] Here, this framework is used to study the conformations and dynamics of the spin label R1 at positions 72 and 131 in T4L. For the first time, very good agreement with multifrequency ESR experiments at three different magnetic field strengths is obtained. The atomically detailed picture of the spin label emerging from the MD simulations helps to unify spectroscopic and crystallographic data and provides useful insight into their molecular origins.

2. Results

2.1. Spectra of 72R1 and 131R1 in T4 Lysozyme. Extensive, all-atom MD trajectories of fully solvated, spin-labeled T4L were used to construct Markov models of 72R1 and 131R1. Models with 37 and 38 states, respectively, provided a temporal resolution of about 160 ps, needed for the calculation of ESR spectra at high fields[24] (Table 1). These states are characterized not only by the five dihedral angles but also by other degrees of freedom of T4L that interact cooperatively. The relaxation time scales of the models as a function of lag time are shown

(12) Barnes, J. P.; Liang, Z.; Mchaourab, H. S.; Freed, J. H.; Hubbell, W. L. *Biophys. J.* **1999**, *76*, 23298.

(13) Langen, R.; Oh, K. J.; Cascio, D.; Hubbell, W. L. *Biochemistry* **2000**, *39*, 8396.

(14) Columbus, L.; Kalai, T.; Jeko, J.; Hideg, K.; Hubbell, W. L. *Biochemistry* **2001**, *40*, 3828.

(15) Guo, Z. Ph.D. Thesis, University of California, Los Angeles, 2003.

(16) Liang, Z.; Lou, Y.; Freed, J. H.; Columbus, L.; Hubbell, W. L. *J. Phys. Chem. B* **2004**, *108*, 17649.

(17) Guo, Z.; Cascio, D.; Hideg, K.; Kalai, T.; Hubbell, W. L. *Protein Sci.* **2007**, *16*, 1069.

(18) Fleissner, M. R. Ph.D. Thesis, University of California, Los Angeles 2007.

(19) Jiao, D.; Barfield, M.; Combarzia, J. E.; Hruby, V. J. *J. Am. Chem. Soc.* **1992**, *114*, 3639.

(20) Meirovitch, E.; Nayeem, A.; Freed, J. H. *J. Phys. Chem.* **1984**, *88*, 3454.

(21) Polimeno, A.; Freed, J. H. *Adv. Chem. Phys.* **1993**, *83*, 89.

(22) Polimeno, A.; Freed, J. H. *J. Phys. Chem.* **1995**, *99*, 10995.

(23) Sezer, D.; Freed, J. H.; Roux, B. *J. Phys. Chem. B* **2008**, *112*, 5755.

(24) Sezer, D.; Freed, J. H.; Roux, B. *J. Chem. Phys.* **2008**, *128*, 165106.

(25) Stoica, I. *J. Phys. Chem. B* **2004**, *108*, 1771.

(26) DeSensi, S. C.; Rangel, D. P.; Beth, A. H.; Lybrand, T. P.; Hustedt, E. J. *Biophys. J.* **2008**, *94*, 3798.

(27) Steinhoff, H.-J.; Hubbell, W. *Biophys. J.* **1996**, *71*, 2201.

(28) Sale, K. L. Ph.D. Thesis, The Florida State University, 2002.

(29) Budil, D. E.; Sale, K. L.; Khairy, K. A.; Fajer, P. G. *J. Phys. Chem. A* **2006**, *110*, 3703.

(30) Beier, C.; Steinhoff, H.-J. *Biophys. J.* **2006**, *91*, 2647.

(31) Sezer, D.; Freed, J. H.; Roux, B. *J. Phys. Chem. B* **2008**, *112*, 11014.

Table 1. Number of Transitions between the m and p Conformations Observed in the MD Trajectories and the Number of Markov States Assigned to Those Conformations[a]

	no. of transitions		no. of states			
site	m → p	p → m	m	p	total	m:p
72R1	2	1	18	19	37	27:73
131R1	1	1	19	19	38	55:45

[a] The m:p ratio (%) is determined from independent restrained simulations, with estimated uncertainties of ±4% for 72R1 and ±12% for 131R1.
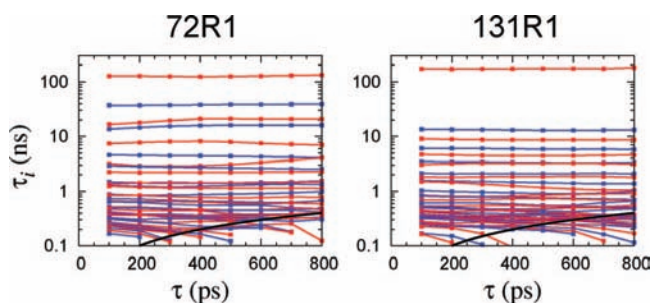

Figure 2. Relaxation time scales $\tau_i(\tau) = -\tau/\ln \lambda_i(\tau)$, implied by the eigenvalues, $\lambda_i(\tau)$, of the transition probability matrices estimated from the data at various lag times τ. The thick black curves correspond to 2τ. τ_i's that fall under these curves are essentially zero and are poorly estimated.

in Figure 2. The fact that the lines are approximately horizontal (i.e., independent of the lag time) indicates that the time series for dihedral dynamics of both 72R1 and 131R1 are faithfully modeled by a Markov model on time scales larger than the lag time.[31] At both sites, the slowest relaxation times ($\tau_1 \gtrsim 100$ ns) are related to transitions of the disulfide torsion angle between its two stable conformations $\chi_3 \approx -90°$ (m) and $\chi_3 \approx 90°$ (p). The exact numerical values of τ_1, as well as the relative populations of the m and p conformations are not expected to be accurately estimated by the constructed Markov model due to the small number of such transitions observed in the free simulations (Table 1). Nevertheless, since τ_1 falls beyond the time scale relevant for ESR experiments at 9 GHz and especially at higher frequencies, its precise value is immaterial for the calculation of such spectra. The spectra can be simulated as a linear superposition of the separate contributions from the m and p conformations weighted by their relative population.[23] To determine accurately the m:p ratio, the free energy difference between two Markovian states on the opposite side of the χ_3 torsion was calculated using umbrella sampling simulations.[32] This resulted in 27% m − 73% p (±4%) for 72R1, and 55% m − 45% p (±12%) for 131R1 (Table 1).

ESR spectra for three different magnetic field strengths were simulated, as described in Methods. The calculated spectra are compared with experiment in Figure 3. [Experimental ESR spectra of 72R1 and 131R1 at 0.33 T (9 GHz) and 8.9 T (250 GHz) have been published previously.[16] In this study, we make use of unpublished newer data for 0.33 T (9 GHz), 3.4 T (95 GHz) and 6.1 T (170 GHz) with improved signal-to-noise that has been provided with permission from Zhang, Fleissner, Hubbell and Freed (to be published).] The spectra calculated by using separately the m and p sub-blocks of the estimated transition probability matrices are shown in the left column, and the final ESR spectra, obtained by linearly mixing the m and p free induction decay curves, in the right column of Figure
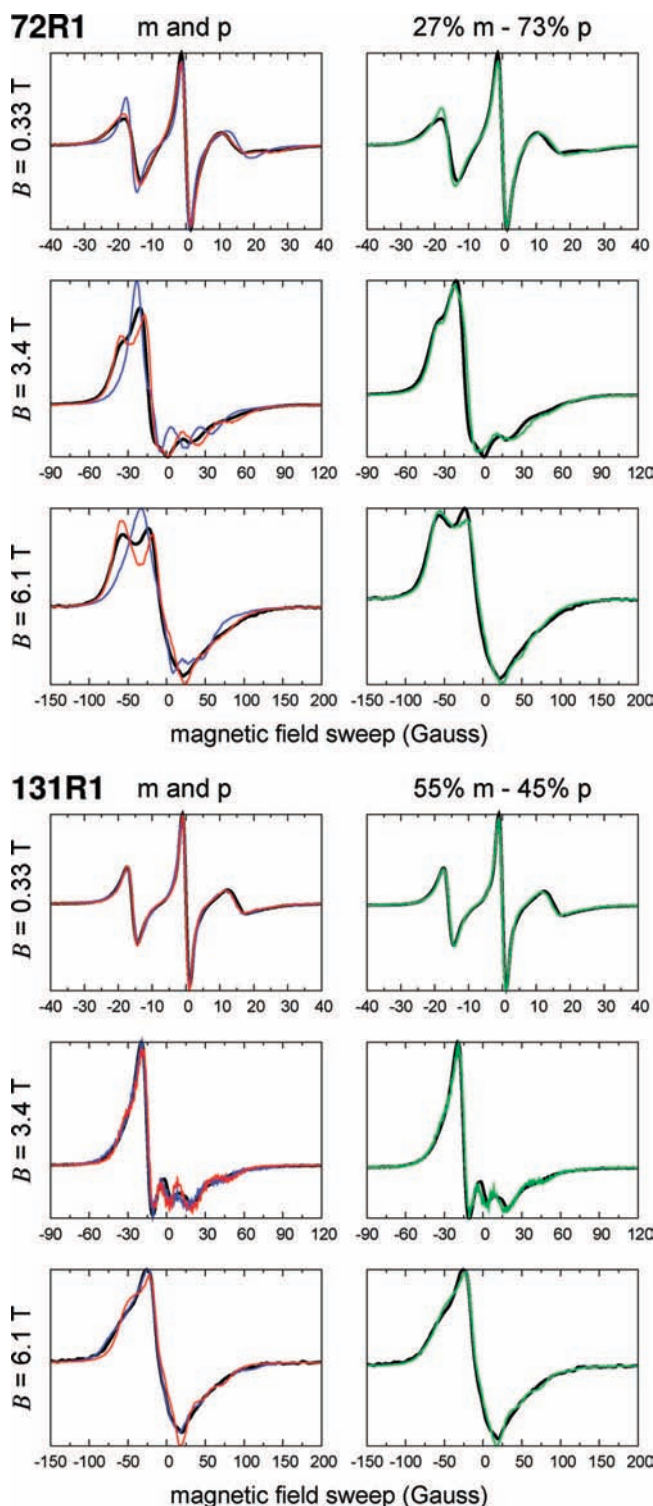
(32) Roux, B. *Comput. Phys. Commun.* **1994**, *91*, 275.

Figure 3. Experimental spectra (black) of 72R1 (top) and 131R1 (bottom) at 22 °C are compared with (left) calculated spectra of the m (blue) and p (red) conformations; (right) spectra calculated by mixing the m and p conformations in the given ratio and adjusting the Lorentzian broadening (green). The simulation parameters are given in Table 7. Experimental spectra are from Zhang, Fleissner, Tipikin, Earle, Hubbell, and Freed (unpublished) by permission.

3. For the three fields, the spectra from the m and p conformations of 131R1 are quite similar to each other and to the experimental spectra, with the difference increasing slightly with the increase of the field (Figure 3, bottom). The agreement between the calculated and the experimental spectra is remark-
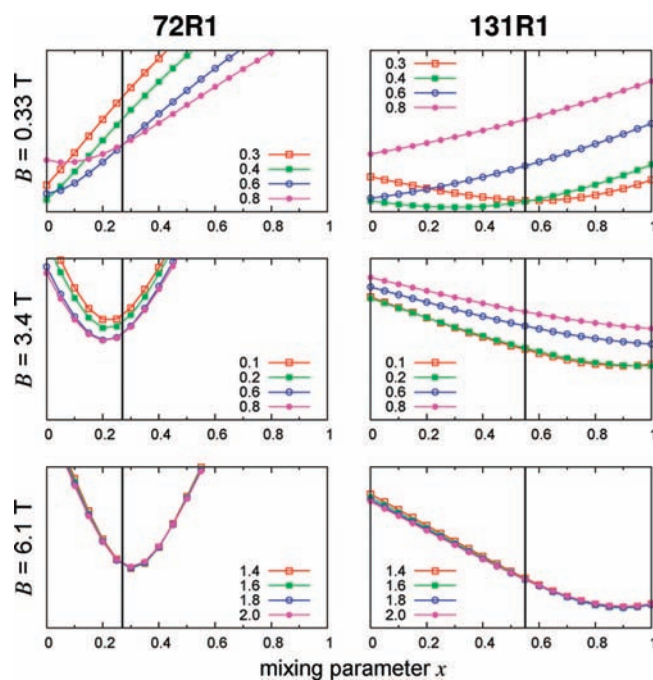
Figure 4. Root-mean-square deviation between the experimental and calculated spectra (arbitrary units), as a function of the weight of the m component ($0 \leq x \leq 1$), for four different choices of the Lorentzian broadening (Gauss). The vertical black lines correspond to the m:p ratio determined from the umbrella sampling calculations and used in the simulation of the spectra in Figure 3.

Table 2. Five Most Populated States of the Markov Model of 72R1 Accounting for 68% of the Total Probability; Dihedral Angles (in deg) for Two of the Most Probable Microstates Belonging to Each State Are Shown; State and Microstate Populations (%) Are π and π_m, Respectively

state	π	π_m	χ_1	χ_2	χ_3	χ_4	χ_5
1	22.3	20.8	−176	49	93	−82	100
		1.3	−170	54	102	−65	97
2	15.7	10.6	−168	48	85	−159	−70
		2.9	−169	54	85	−169	−81
3	13.7	4.0	−169	48	78	−144	20
		3.8	−162	47	79	−170	88
4	8.7	4.0	−63	−66	94	172	57
		1.8	−65	−78	84	145	87
5	7.4	1.2	−55	−44	−91	−178	−93
		1.1	−57	−37	−87	−171	−7

analysis of the spin-label conformations, in an effort to understand the molecular origins of the observed ESR spectra.

2.2. Conformations and Dynamics of R1 at Sites 72 and 131. The most populated five states of 72R1 from the Markov model are presented in Table 2, and the corresponding spin-label conformations are shown in Figure 5A. In spite of the variation of χ_4 and χ_5, as well as χ_1, χ_2, and χ_3, across the most populated states, the nitroxide ring appears to be rather well localized (Figure 5A). In contrast, the conformations corresponding to the first five most populated states of 131R1 (Table 4) are more diffuse (Figure 5B). To clarify the causes of such spin-label behavior in the MD simulations, we calculated the interaction energies between the nitroxide ring, including C_ε and S_δ, and the neighboring amino acid residues, both side chain and backbone atoms (Tables 3 and 5). It is important to keep in mind that the nitroxide is an amphipathic polar−nonpolar moiety (with hydration free energy about −2.0 kcal/mol), seeking out hydrophobic pockets and favorable electrostatic environments.

For 72R1 favorable van der Waals (vdW) contacts with the hydrophobic residues Phe4, Val75, Val71, and Ile3 are observed (Table 3). Even the interactions with the polar Asn68 and the charged Arg76, when present, are mainly nonelectrostatic. This result offers an explanation of why alanine mutations at positions $i \pm 3$ and $i \pm 4$ did not detect interactions of the spin label with its neighbors.[10,11] First, residue $i -1$ and amino acids distant in the sequence are involved in the interactions. Second, alanines at positions $i -4$ (N68A) and $i +3$ (V75A) can also engage in nice hydrophobic contacts with R1 both in the m and p states, as we have found in MD simulations in the context of R1 on a polyalanine α-helix.[23] The prevalence of the p conformations for 72R1 is consistent with the observation that the m states cannot establish vdW interactions with Ala at position $i -1$, whereas the p states interact best with that position.[23]

At position 131 the spin label is found to participate in interactions that are varied, both in nature and in the identity of the partner (Table 5). Since the electrostatic interactions were calculated in vacuum, the relatively large interaction energies with distant amino acids appearing in this table are in fact less significant in the presence of water. The values are more representative when the spin label and its partner are in proximity, which can be inferred from the presence of a significant vdW interaction. Therefore, in Table 3 relatively large electrostatic interactions were highlighted only when the corresponding vdW interactions were also significant (i.e., larger than k_BT). Interestingly, in its dominant state R1 is involved in

ably good over the entire field range. In the case of 72R1, the m and p contributions to the spectra are markedly different, with the latter being consistently more similar to the experimental spectrum for all the three field strengths (Figure 3, top). At 0.33 T (9 GHz), the p component by itself is basically identical to the experimental spectrum, whereas adding 27% of the m component is essential for the good agreement at the two higher fields.

In Figure 4 we show the root-mean-square deviation (rmsd) between the calculated and the experimental spectra over the full range of m:p ratios, obtained by changing the weight, x, of the m component (and therefore also the weight $1 − x$ of the p component). The plots reveal that the ratio calculated using umbrella sampling simulations is consistently close to what would be the optimal choice if x were adjusted empirically to best-fit the experimental spectra. Although it appears that for 131R1 a combination of about 80% m − 20% p would lead to better agreement with experiment, the resulting decrease in the rmsd (shown in Figure 4), is actually insignificant. This is clear by comparing the m and p spectra of 131R1 in Figure 3 (left column). The two spectra are sufficiently similar that almost any choice of x in the entire range from 0 to 1 yields an acceptable spectrum.

By changing the ESR frequency from 9 to 170 GHz the time window of sensitivity of the experiment is changed by about an order of magnitude. Also, whereas at 9 GHz the spectrum is dominated by the hyperfine tensor, at 95 GHz the contribution of the **g** tensor becomes more significant, and eventually dominates at 170 GHz. Therefore, the quantitative agreement of the calculated spectra with experiment over the 9−170 GHz range is strongly suggestive that the dynamics of the spin label in the computer simulations is quite similar to the real underlying dynamics. As a result, we consider the structural and energetic
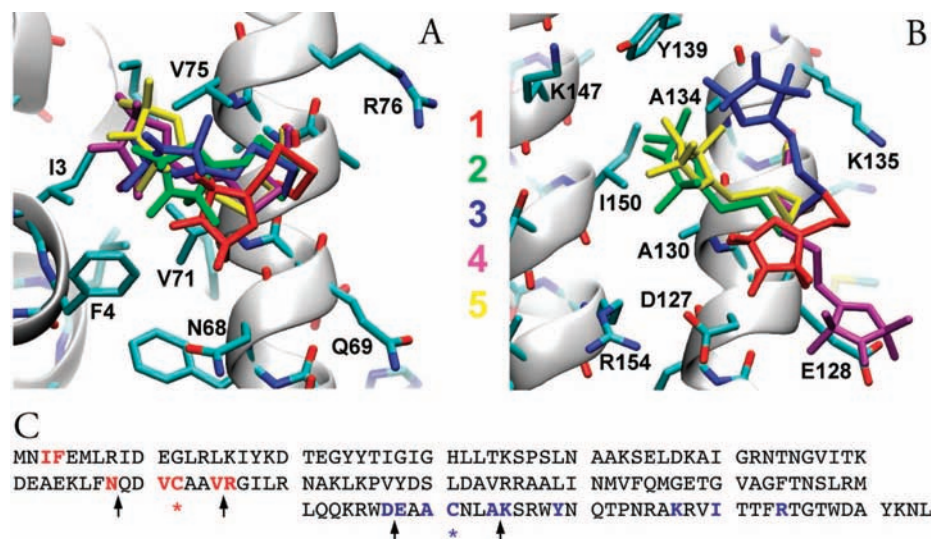
Figure 5. Most populated five conformations of 72R1 (A) and 131R1 (B) are colored as indicated. The rotameric states of the neighboring side chains when interacting with R1 are not necessarily the same as the ones shown here. (C) Amino acid sequence of T4L. Stars indicate the spin-labeled sites, and arrows point between the $i \pm 3$ and $i \pm 4$ positions. Residues with which R1 interacts are colored red and blue for 72 and 131, respectively.

Table 3. Interaction Energies (kcal/mol) with the Specified Residues for the First Five States of 72R1; van der Waals (vdw) and Electrostatic (elec) Contributions Are Shown Separately; Energies Larger than the Thermal Energy at Room Temperature (0.6 kcal/mol) Are in Bold

state		I3	F4	N68	V71	V75	R76
1	vdw	−0.2	**−1.3**	**−1.7**	**−1.6**	**−1.5**	**−1.7**
	elec	−0.3	−0.6	0.2	0.0	−0.1	**1.1**
	total	−0.5	**−1.9**	**−1.5**	**−1.6**	**−1.7**	−0.6
2	vdw	−0.5	**−1.4**	−0.5	**−1.2**	**−2.2**	**−1.2**
	elec	−0.5	−0.2	−0.3	0.2	−0.1	**0.7**
	total	**−1.0**	**−1.6**	**−0.7**	**−1.0**	**−2.3**	−0.5
3	vdw	**−0.7**	**−1.5**	−0.4	**−1.1**	**−2.2**	**−1.2**
	elec	0.0	−0.1	−0.3	0.2	0.1	0.6
	total	**−0.7**	**−1.6**	**−0.7**	**−0.9**	**−2.1**	**−0.7**
4	vdw	**−0.8**	**−1.6**	−0.5	**−1.6**	**−2.1**	−0.4
	elec	0.0	0.0	−0.5	0.1	0.4	**1.0**
	total	**−0.8**	**−1.6**	**−1.0**	**−1.5**	**−1.7**	0.5
5	vdw	**−0.9**	**−1.7**	−0.5	**−1.4**	**−2.0**	−0.3
	elec	0.0	0.1	0.2	−0.4	0.3	1.5
	total	**−0.8**	**−1.6**	−0.3	**−1.8**	**−1.7**	**1.2**

Table 4. Five Most Populated States of the Markov Model of 131R1 Accounting for 60% of the Total Probability; States That Agree with Either of the Two (χ_1, χ_2) Values Observed in a Recent Crystal Structure[18] Are Indicated with Daggers

state	π	π_m	χ_1	χ_2	χ_3	χ_4	χ_5
1	18.6	17.3	−173	173	−96	72	−100
		0.8	−171	−132	−102	74	−98
2[†]	18.1	8.1	−62	−48	101	−161	77
		5.4	−62	−53	102	−169	53
3[‡]	7.9	3.9	−171	66	−97	174	−63
		1.2	−171	73	−91	−159	−82
4	7.9	4.8	−65	−177	−84	−174	−87
		1.8	−70	−178	−95	174	−70
5[†]	7.2	2.9	−58	−58	97	173	−83
		1.9	−61	−60	97	163	−23

Table 5. Interaction Energies (kcal/mol) of the First Five States of 131R1 with the Specified Residues; van der Waals (v) and Electrostatic (e) Contributions to the Total (t) Energy Are Shown Separately

		D127	E128	A130	A134	K135	Y139	K147	I150	R154
1	v	**−2.4**	**−1.5**	**−0.8**	−0.1	−0.4	0.0	0.0	−0.1	**−1.8**
	e	**4.3**	0.6	−0.2	0.1	0.8	0.3	0.3	0.1	**−4.5**
	t	**1.9**	**−1.0**	**−1.0**	−0.1	0.4	0.2	0.3	0.0	**−6.3**
2[†]	v	**−0.7**	−0.2	**−2.0**	**−1.2**	−0.2	**−1.5**	**−1.7**	**−1.6**	**−1.6**
	e	**−2.7**	−0.7	0.2	0.4	0.4	0.1	**−5.4**	−0.1	**2.0**
	t	**−3.3**	**−0.9**	**−1.8**	**−0.8**	0.1	**−1.4**	**−7.1**	**−1.7**	0.3
3[‡]	v	−0.1	−0.1	−0.4	**−1.8**	**−2.2**	**−1.4**	−0.2	−0.2	−0.1
	e	−0.6	**−2.1**	−0.4	**0.7**	**2.6**	0.3	−0.2	0.1	0.3
	t	**−0.7**	**−2.2**	**−0.8**	**−1.1**	0.4	**−1.1**	−0.3	0.0	0.2
4	v	**−1.9**	**−2.7**	−0.2	0.0	−0.1	0.0	0.0	0.0	−0.2
	e	**−1.9**	**−2.7**	0.2	−0.1	0.6	0.1	0.4	1.3	1.3
	t	**−3.8**	**−5.5**	0.0	−0.2	0.5	0.1	0.4	**1.3**	**1.0**
5[†]	v	**−0.6**	−0.2	**−1.7**	**−1.0**	−0.3	**−1.2**	**−1.0**	**−1.0**	**−1.6**
	e	**−1.9**	−0.9	0.1	0.5	0.4	0.2	**−4.7**	−0.1	**1.8**
	t	**−2.5**	**−1.1**	**−1.6**	−0.5	0.1	**−1.0**	**−5.8**	**−1.1**	0.2

Asp127. The ability of R1 to participate in diverse (hydrophobic and electrostatic) interactions simultaneously with several partners, suggests that alanine mutations at nearby $i \pm 3$ and $i \pm 4$ positions may not result in drastic changes, especially since both the m and p conformations of R1, deduced to be almost equally populated at position 131, were observed to establish favorable vdW contacts with alanines at those positions.[23]

The character of the dynamics that underlies the calculated spectra can be examined from the trajectories. Such dynamics is rather complex and affected by the interactions of the spin label with the solvent and the protein. Torsions about χ_5 are the most rapid. They occur almost every $1-2$ ns, though transition times can be on the order of 10 ns for some rotamers. Such rapid kinetics of χ_5 is consistent with the low energetic barrier ($1-2$ kcal/mol).[23] Transitions of χ_4 can also be as fast as a few nanoseconds, but sometimes as slow as tens of nanoseconds, depending on the rotameric state of the spin label. Similarly, the transitions associated with χ_2 and χ_1 occur on a range of time scales spanning from a few nanoseconds to tens of nanoseconds. In contrast, transitions about the χ_3 dihedral

favorable electrostatic and vdW interactions with Arg154. The interaction energy remains significant even after accounting for the unfavorable electrostatic and favorable vdW interactions with

occur much more infrequently, mainly due to the large energy barrier around the disulfide bond separating the rotameric states of the spin label into two classes of conformations, m and p.

3. Discussion

ESR spectra were generated from stochastic simulations based on discrete-state Markov jump models whose parameters were extracted from all-atom MD trajectories. Thus, these states are characterized by the all-atom degrees of freedom, from which the orientations of the five dihedral angles are obtained.[31] This strategy was developed to optimally exploit the information contained in the MD simulations and also circumvent the need for exceedingly long (~ 1 μs) continuous trajectories, required to simulate ESR spectra. Following this procedure, continuous-wave ESR spectra at three magnetic field strengths were calculated for sites 72 and 131 in T4 Lysozyme (T4L). Although the Markov models were constructed to reflect the time-series of the five spin-label torsion angles, the influence of the environment is incorporated in two ways. First, the electrostatic and van der Waals interactions with the protein and the solvent molecules dictate which rotameric states of the spin label are populated and to what extent. Due to the internal flexibility and amphiphilic nature of the spin label, the populations of its conformations result from the detailed balance between various interactions.[23] Such populations would be hard to predict on the basis of simplified steric and hydrodynamic arguments.[33] Second, explicit protein and solvent dynamics on time scales up to about 100 ps was used to calculate preaveraged magnetic tensors for each of the states of the Markov models. Therefore, the fast rattling of the nitroxide in the solvent cage and the local thermal fluctuations of the protein backbone (as opposed to larger-scale conformational changes, e.g. partial unfolding of the helices, etc.), are implicitly accounted for in the spectral simulations, in addition to the exchange between the rotamers.

In the simulations the spin label attached to the protein can adopt a multiplicity of conformations, many of which tend to interconvert on time scales relevant for ESR experiments. When the exchanges are slow, the states appear to be stabilized by a range of interactions frequently involving the nitroxide ring. An important consequence of the slow interconversion rate of the χ_3 torsion about the disulfide bond is that all calculated spectra are actually a simple linear superposition of individual m ($\chi_3 \approx -90°$) and p ($\chi_3 \approx 90°$) spectral components, weighted by the equilibrium population ratio (m:p) of those two states. As observed in Figure 3, when the m and p spectral components differ significantly, the particular value of the m:p ratio used to produce the final spectra is critical to the good agreement with the experimental spectra. In the present study, the equilibrium m:p ratios were calculated for 72R1 and 131R1 via umbrella sampling simulations. This strategy was utilized to overcome the poor statistics in the spontaneous isomerization of the χ_3 dihedral angle in free unbiased MD trajectories. As we have noted above (see also Figure 4) adjusting the m:p ratio empirically to best fit the experimental spectra yields values very similar to the umbrella sampling results, indicating the utility of this method. It also provides further support for the MD results.

It is important to emphasize that the atomistic MD trajectories yield considerably more detail than can be discerned in actual experiments. According to the simulations, the dynamics of R1

at site 72 and 131 involves jumps between different rotameric states. However, due to the complex interplay of interconversion rates, this tumultuous complexity remains largely hidden at the level of the observed spectra. Obviously, a wide range of possible microscopic dynamics could yield similar spectra. For example, although the m and p conformations of 131R1 correspond to different families of rotamers by definition, they yield essentially identical 9 GHz spectra (see Figure 3). Thus, a unique dynamical model cannot be inferred on the basis of 9 GHz spectra alone. Multifrequency ESR analysis attempts to address this issue by placing additional restrictions on the nature of the microscopic dynamics. The constraints presented by multifrequency spectra are important, e.g., a single diffusional model MOMD is unable to simultaneously fit both the low- and high-frequency spectra from T4L.[12,16] Achieving a simultaneous agreement is challenging even for state-of-the-art fitting approaches based on the SRLS model, which also raises the question of uniqueness of fit, even with the additional restrictions imposed by multifrequency ESR.[12,16,34] However, the present results, which have yielded spectra in excellent agreement with experiment at three different frequencies, were generated from a single microscopic model of the dynamics without adjusting or fitting any parameters. Nevertheless, the great difficulty to infer a unique model of microscopic dynamics from spectral analysis should be kept in mind when trying to reconcile the present results with traditional discussions of spin-label dynamics.

Spin labels attached to position 72 and 131 in T4L have been used in several previous experimental studies to characterize the spin-label dynamics at solvent-exposed helix surface (SEHS) sites.[14,18] The latter are positions where the spin label makes no nearest-neighbor or tertiary interactions. In fact, according to the MD results illustrated in Figure 5, the spin labels at 72 and 131 can interact with distant residues in the protein. This implies that those positions are not, strictly speaking, "true" SEHS sites. The dynamical behavior of spin labels attached at SEHS sites has been encapsulated into the so-called χ_4/χ_5 model.[2] According to the χ_4/χ_5 model, the last two dihedrals, χ_4 and χ_5, undergo rapid isomerization dynamics, while the dihedrals χ_1, χ_2 and χ_3 remain essentially "locked" around well-defined conformations on the time scale of the ESR experiments. The restricted motion of the spin label leads to an anisotropic dynamics that can be characterized by just a single-order parameter and an effective correlation time, in close correspondence with the fitted parameters of the MOMD model in spectral simulations, at 9 GHz in viscous medium.

Consistent with the χ_4/χ_5 model, only specific combinations of χ_1 and χ_2 have indeed been observed in a number of X-ray crystallographic structures of spin-labeled T4L.[15,18,35] The atoms beyond the second sulfur S_δ are typically unresolved in the electronic density, and the conformations of R1 are represented in terms of the dihedral angles χ_1 and χ_2 with $t = 180°$ and $g^\pm = \pm 60°$. The observed conformations in X-ray structures of T4L are g^-g^-, tg^+, tg^-, g^-t[15,35] (see Table 3-1 in ref 18). Specific interactions have been proposed to explain the high propensity of those conformations,[13,15] in particular, a hydrogen bond between S_δ and the backbone H_α is thought to stabilize the g^-g^- and tg^+ rotamers (see Figure 1, top).[13] The rotamers occurring with the highest frequency in the MD simulations, given in Tables 2 and 4 for 72R1 and 131R1, respectively, are generally in reasonable accord with the available structural data from

(33) Tombolato, F.; Ferrarini, A.; Freed, J. H. *J. Phys. Chem. B* **2006**, *110*, 26248.

(34) Liang, Z.; Freed, J. H. *J. Phys. Chem. B* **1999**, *103*, 6384.
(35) Langen, R.; Oh, K. J.; Cascio, D.; Hubbell, W. L. *Biochemistry* **2000**, *39*, 8396.

X-ray crystallography. For example, the five states in Table 2 accounting for 68% of the total probability for 72R1, correspond to tg^+ and g^-g^-, which have also been observed in X-ray structures of spin-labeled T4L. In the case of 131R1, the five states in Table 4, which account for 60% of the total probability, correspond to g^-g^-, tg^+, tt, and g^-t. The first two of these rotamers were seen in a recent crystal structure of T4L labeled at site 131,[18] whereas the tt and g^-t conformations were not observed. Since each of the latter rotamers represent less than 20% of the total probability in the MD simulations (Table 4), it seems plausible that they could remain undetected in X-ray diffraction experiments. It is also possible that their actual populations are smaller than the results in Table 4. Of particular interest is the rotamer tt, which occurs transiently during the simulations but has not been observed (so far) in X-ray structures of spin-labeled T4L. We can offer no obvious reason why this rotamer should not occur since it is not prohibited by any steric clash. In fact, we note that electron nuclear double resonance (ENDOR) experiments indicate that it is one of the dominant conformations for an MTSSL spin label attached to TEM-1 β-lactamase in solution.[36]

The above comparison indicates that, while there is no exact correspondence, the χ_1 and χ_2 rotameric states found in the MD simulations are reasonably consistent with the available structural data used to support the χ_4/χ_5 model. In contrast, the complex dynamics of the spin label emerging from the MD trajectories and the Markov analysis does depart significantly from the perspective drawn from the χ_4/χ_5 model. Although the most rapid transitions involve the last torsion χ_5 in accord with this model, considerable differences exist with regard to the dihedrals χ_1 and χ_2. In this case, isomerizations occur over a range of time scales spanning from a few nanoseconds to tens of nanoseconds, which overlap with the ESR time scale. In particular, the 9 GHz spectra typically become sensitive to motions faster than about 100 ns, whereas for the higher frequencies, it is closer to 10 ns. The particular isomerization rates depend on the specific rotameric states, a feature that is observed also for χ_4 and χ_5. The hydrogen bond between S_δ and the H_α, playing an important role in the context of the χ_4/χ_5 model, is indeed observed in the MD, though the interaction appears to be too weak ($\sim$1 kcal/mol) to immobilize the spin label on the ESR time scale. Although the present simulations rely on approximations, which could somewhat affect the populations of the conformers in Tables 2 and 4, the microscopic interactions involving the spin label (carefully parametrized on the basis of extensive ab initio calculations[23]) should be described rather accurately.

The isomerizations of χ_1 and χ_2 occurring on the ESR time scale in the MD may seem incompatible with the experimental evidence presented in support of the χ_4/χ_5 model. For example, the 9 GHz ESR spectra of 72R1 and 131R1 can indeed be simulated using MOMD for the restricted motion implied by the χ_4/χ_5 model. However, the same spectra are also reproduced accurately with the complex spin-label dynamics arising from the MD trajectories, as shown in Figure 3. As pointed out above, agreement with 9 GHz spectra is insufficient to prove the uniqueness of a dynamical model. On the other hand, the MD trajectories have been performed only for the case of a single temperature and simple aqueous solvent.

The ability of the spin label to adopt a multitude of rotameric states and undergo isomerization transitions on the nanosecond time scale seen in MD is consistent with modern views of protein dynamics. Rather than being exceptional, side-chain disorder, polymorphisms, and isomerization dynamics are pervasive phenomena in proteins.[37,38] Even structural features that are well resolved in X-ray structures can display inherent fluctuations. A classical example is the tyrosine side chain in BPTI, where a buried side chain has the ability to undergo rapid isomerization.[39]

Given the success in fitting the multifrequency ESR spectra shown in Figure 3, it would be worthwhile to attempt further MD simulations to cover a range of temperatures (and possibly solvents) to further test their ability to predict ESR spectra under different conditions. Also, we note that, although great care was taken in the development of force fields used, it would be of interest to evaluate the effects of small variations, given the subtle interplay of various interactions that yielded the results described above. (One key detail is the use of the well-known but *ad hoc* time-scale factor to correct the viscosity of nonpolarizable waters in MD simulations.[40]) A physically relevant aspect, worthy of further study, suggested by the Markov models, is the extent of cooperativity of the R1 side-chain dynamics with the other degrees of freedom, such as backbone motions.

Spectral fits with the MOMD or SRLS models play a very useful role in the analysis of experimental spectra. These models help to quantify a large variety of spectral line shapes in terms of a few parameters (the order tensors and the rotational diffusion tensors), which are easier to report and to compare. Nevertheless, the need to account for dynamics that are more complex than the MOMD model has long been recognized.[2] The Markov jump model that we constructed from the MD simulations represents one possible step in this direction. It can be viewed as a natural extension of the multicomponent SRLS model in which the spin-label dynamics includes a number of components (i.e., randomly distributed orientations of the nitroxide moieties), each with their own microscopic order tensors. It is our hope that the overall perspective developed from the MD simulations can help design better motional models tailored to the specific spin label and biomolecule to which it is attached. Going beyond a universal, generic stochastic model is expected to be of crucial importance, given the extensive applications of SDSL to diverse biological systems and the increased availability of high-field ESR methods.

4. Methods

4.1. MD Simulations and Construction of the Markov Models. The MD simulations were performed with the program CHARMM,[41] using the CHARMM22 protein force field[42] with CMAP correction.[43] The electrostatics was treated with particle

(36) Mustafi, D.; Sosa-Peinado, A.; Gupta, V.; Gordon, D. J.; Makinen, M. W. *Biochemistry* **2002**, *41*, 797.

(37) Frederick, K. K.; Marlow, M. S.; Valentine, K. G.; Wand, A. J. *Nature* **2007**, *448*, 325.

(38) Igumenova, T. I.; Frederick, K. K.; Wand, A. J. *Chem. Rev.* **2006**, *106*, 1672.

(39) McCammon, J. A.; Karplus, M. *Proc. Natl. Acad. Sci. U.S.A.* **1979**, *76*, 3585.

(40) Bogusz, S.; Venable, R. M.; Pastor, R. W. *J. Phys. Chem. B* **2001**, *105*, 8312.

(41) Brooks, B. R.; Bruccoleri, R. E.; Olafson, B. D.; States, D. J.; Swaminathan, S.; Karplus, M. *J. Comput. Chem.* **1983**, *4*, 187.

(42) MacKerell, A. D., Jr.; et al. *J. Phys. Chem. B* **1998**, *102*, 3586.

(43) MacKerell, A. D., Jr.; Feig, M.; Brooks, C. L. *J. Comput. Chem.* **2004**, *25*, 1400.

Table 6. Information about the Two Sets of MD Simulations[a]

	set 1	set 2
labeled sites	**72**, 44, 109, 119	**131**, 40, 69, 82
number of indep. traj.	18 (χ_1, χ_2, χ_3)	54 (χ_1, χ_2, χ_3, χ_4)
duration of a single traj.	32.3 ns	12.7 ns
total sim. time (analyzed)	581 (563) ns	686 (632) ns

[a] In each independent trajectory of a given set the spin labels were initialized to be in a different rotameric state by restraining the indicated dihedral angles (in parenthesis) to their local minima. The multiplicity of the dihedral angles, which determines the number of different rotamers, is χ_1:3, χ_2:3, χ_3:2, and χ_4:3.

Table 7. Parameters Used in the Simulation of the ESR Spectra at the Specified Field/Frequency (B/f)[a]

				T_L^{-1} (G)	
B (T)	f (GHz)	stpN	sphN	72R1	131R1
0.33	9.4	3000	800	0.7	0.35
3.40	95	2500	25600	0.75	0.1
6.10	170	2000	25600	1.6	1.8

[a] The diffusive tumbling of the macromolecule with respect to the lab-fixed frame was initialized from 'sphN' spherical grid points; 200 stochastic trajectories lasting for 'stpN' steps were launched from each grid point. A simulation time step of 200 ps was used with the Markov transition matrices estimated at $\tau = 100$ ps, where the 2-fold difference aims to correct for the unrealistically low viscosity of the TIP3P water model used in the MD simulations. T_L^{-1} is the Lorentzian broadening, introduced in the simulations by hand, yielding best agreement with experiment.

Table 8. Magnetic Tensors Used in the Simulations[a]

site	g_{xx}	g_{yy}	g_{zz}	A_{xx}	A_{yy}	A_{zz}
72R1	2.00809	2.00585	2.00202	6.2	4.3	36.2
131R1	2.00811	2.00586	2.00202	6.0	4.1	37.0

[a] Provided by Z. Zhang; see also ref 16.

mesh Ewald summation.[44] The parameters not available in the existing force field were optimized targeting the electrostatic and energetic properties of MTSSL determined from *ab initio* calculations.[23] The simulated system consisted of a spin-labeled T4L, together with 7305 TIP3P water molecules, and 11 sodium and 19 chloride counterions. Two different sets of simulations were performed at $T = 297$ K and $P = 1$ atm. In one of the sets, 18 trajectories were simulated for 32.3 ns; in the other, 54 trajectories were simulated for 12.7 ns. The first one ns was excluded from the analysis. In the first set, T4L was labeled at sites 44, 72, 109, and 119; in the second, at sites 40, 69, 82, and 131 (Figure 1). The spin label was initiated in a different rotameric state in each of the independent trajectories. This information is summarized in Table 6.

The MD trajectories were mapped to a stochastic jump model of the R1 dynamics by using the values of its five dihedrals to infer the states of the (hidden) Markov model and estimate a transition matrix of the state-to-state jump probabilities.[31] Because of the relatively limited duration of each MD trajectory, only one transition was observed out of some states with $\chi_1 \approx 60°$ as if R1 can never return to these states. This value of χ_1 is known to be unfavorable for S_γ when R1 is on α-helices. (Only 5% of cysteines on helices have been observed to adopt this conformation in crystal structures.[45]) Entirely discarding such low probability states might not necessarily be a bad approximation, but we decided to introduce one artificial transition that enters those states from the state that they exited to when constructing the transition probability matrix.

(44) Essmann, U.; Perera, L.; Berkowitz, M. L.; Darden, T.; Lee, H.; Pedersen, L. G. *J. Chem. Phys.* **1995**, *103*, 8577.
(45) Lovell, S. C.; Word, J. M.; Richardson, J. S.; Richardson, D. C. *Proteins* **2000**, *40*, 389.

Similarly, only one transition was observed into one of the m states of 72R1. To prevent this state from acting as a sink, one artificial transition out of this state was introduced. According to the resulting equilibrium probability vector, this state represents 3% of all the m states. Since the m states are calculated to have a population of 27%, even doubling the probability of the uncertain state is not expected to affect the reported results.

For the restrained simulations that were necessary to calculate the m:p ratio, 16 harmonic umbrella potentials were distributed linearly along a path going from one m to one p Markov states, thus crossing the χ_3 dihedral barrier. The sampling was combined with the weighted histogram analysis method[32] and used to calculate the free energy difference (i.e., ratio of probabilities) of the two chosen states. The simulations in each of the umbrellas were run for 6 ns. The first 1 ns was excluded from the analysis. The uncertainties of the relative m and p populations (caption of Table 1) correspond to the standard deviation of the m:p ratio calculated separately from each nanosecond. The absolute uncertainties are expected to be larger due to the additional uncertainties of the probabilities assigned to the states by the constructed Markov model.

4.2. Simulation of the ESR Spectra. To calculate ESR spectra in the time domain, we simulated trajectories of the instantaneous orientation of the nitroxide-fixed coordinate system N, with respect to the laboratory-fixed system of axes L, according to the motional model[24,31]

$$L \xrightarrow{\text{rotational diffusion}} M \xrightarrow{\text{Markov chain}} N \qquad (1)$$

using the parameters presented in Table 7. The components of the magnetic tensors in the nitroxide frame, shown in Table 8, were kindly provided by Z. Zhang (private communication, see also ref 16). The molecular frame M, rigidly attached to the T4L molecule, was modeled to undergo global tumbling with rotational diffusion coefficient $D = 18 \times 10^6$ s^{-1}, which is based on the estimate of a multifrequency ESR study and SRLS fit.[16] The MD trajectories provide detailed representation of the dynamics of N with respect to M. The Markov models constructed from the MD trajectories offer a coarse-grained version of this dynamics but allow us to simulate as many and as long trajectories as required for the convergence of the spectra. Decomposing the dynamics of R1 according to the model (1), requires the definition of a molecular frame, M. The global tumbling of T4L was removed from the MD trajectories by superimposing the MD snapshots such that the deviation of the root-mean-square distance of all the protein backbone atoms was minimized.

For each of the Markovian states, the magnetic tensors were preaveraged over the fast dynamics of N with respect to M using the MD trajectories.[24,31] This was done by calculating the instantaneous magnetic tensors in the molecular frame (attached to the protein) for each snapshot along the MD trajectory and adding those tensors. By adding tensors only from trajectory segments that were in a given Markov state we calculated preaveraged magnetic tensotrs for that state. Such preaveraged magnetic tensors not only reduce the effective diagonal values of the magnetic tensors in the nitroxide frame but also lead to nitroxide frames which have state-dependent orientations with respect to the protein frame. (Naturally, different conformations of the spin label orient the nitroxide frame differently with respect to the protein.) In fact, the state-dependent "nitroxide frame" calculated in this way is different for the **g** and the **A** tensors, since their anisotropies average differently. As a result, for each Markov state we had a g-frame and an A-frame.

Lorentzian broadening was introduced in the simulation of the spectra in Figure 3 (Table 7). When kept within reasonable range, the particular choice of the broadening does not significantly affect the quality of the agreement between the calculated and the

experimental spectra, as demonstrated by their root-mean-square deviation shown in Figure 4.

Supporting Information Available: Complete ref 42. This material is available free of charge via the Internet at http://pubs.acs.org.

JA8073819